Cone Penetration Testing 2022 – Gottardi & Tonni (eds)
© 2022 the Author(s), ISBN 978-1-032-31259-0
Open Access: www.taylorfrancis.com, CC BY-NC-ND 4.0 license

PFEM modeling of CPTu tests in saturated structured soils

Kateryna Oliynyk
School of Science and Engineering, University of Dundee, Dundee, UK
Department of Civil and Environmental Engineering, University of Perugia, Perugia, Italy

Matteo O. Ciantia
School of Science and Engineering, University of Dundee, Dundee, UK

Claudio Tamagnini
Department of Civil and Environmental Engineering, University of Perugia, Perugia, Italy

ABSTRACT: The conventional interpretation of CPTu tests is typically based on empirical and semi-empirical correlations based on very crude descriptions of soil behavior, such as the total stress approach coupled with the Terzaghi-Rendulic pseudo-3d consolidation theory for modeling the time evolution of excess pore water pressure. The aim of this work is to show that a more rational interpretation of the coupled deformation and flow processes occurring in the soil during a CPTu test is possible by resorting to the numerical solution of the relevant governing equations, incorporating a realistic constitutive model for the soil. In order to deal with the large displacements and deformations induced by the cone penetration, the Particle Finite Element Method code G-PFEM, recently developed for geomechanical applications, has been used for this purpose. A key feature of the present work is the use of a finite deformation version of a non-associative isotropic hardening plasticity model for structured geomaterials - the FD_Milan model. The model is equipped with a *structure-related* internal variable which provide a macroscopic description of the effects of structure in natural, fine-grained soils. In order to deal with strain localization, typically observed in structured geomaterials upon yielding, the model has been equipped with a non-local version of the hardening laws, which has demonstrated capable of regularizing the pathological mesh dependence of classical FE solutions in the post-localization regime. A number of PFEM simulations of CPTu tests on a soft structured natural clay has been performed in order to assess the effects of the initial bond strength and permeability on the predicted results of the test, as well as on the spatial distributions of accumulated plastic strains, internal variables and excess pore water pressures. The results obtained represent a promising step towards a more rational interpretation of the CPTu tests in structured geomaterials and for their use in the calibration of advanced soil models.

1 INTRODUCTION

The Cone Penetration Test (CPT) is a widely used investigation tool for the characterization of both coarse-and fine-grained soils, for its simplicity, reliability and its relatively low cost. The development of the piezocone, featuring piezometers for the measurement of pore water pressure p_w at different positions on the cone tip, has significantly improved the capabilities of this site investigation tool - now referred to as CPTu test - and opened the way for a more rational interpretation of the test results.

The conventional interpretation of CPT tests is currently based on empirical and semi-empirical correlations, the last based on very crude descriptions of soil behavior, such as the adoption of a total stress approach. The excess pore pressure measurements in CPTu tests are typically used to identify fine-grained soils (where Δp_w are large) from coarse-grained soils (where Δp_w are small or negligible), or to measure the soil coefficient of consolidation from pore pressure dissipation stages, where the tip advancement is stopped.

The aim of this work is to show that a more rational interpretation of the coupled deformation and flow processes occurring in the soil during a CPTu test is possible by resorting to the numerical solution of the relevant governing equations for the penetration process, and by adopting a realistic constitutive model for the soil. In early attempts to simulate the CPT test with the ALE-FE method, the extreme deformations imposed to the soil by the penetration of the piezocone have represented a substantial difficulty, due to strong mesh distortions which resulted in significant loss of accuracy or loss of convergence at relatively small penetration depths.

DOI: 10.1201/9781003308829-90

An effective alternative to the FEM which has proven to be quite efficient in simulating the cone penetration process is the Particle Finite Element Method (PFEM, Oñate et al. 2011). The PFEM shares many similarities with the updated Lagrangian approach of non-linear FEM, but it is capable of handling the problem of severe mesh distortion by a frequent mesh re-triangulation and *h*-adaptive refinement, using very efficient algorithms based on extended Delaunay tesselation. The nodes of the spatial discretization - performed with low-order linear triangles or tetrahedra - are treated as material particles, the motion of which is tracked during the numerical simulation. Applications of PFEM to the modeling of CPTu tests have been reported, *e.g.*, by Monforte et al. (2017), Monforte et al. (2018), Monforte et al. (2021), Hauser and Schweiger (2021) and Carbonell et al. (2022).

As far as modeling CPTu tests in clays is concerned, most of the works cited have been carried out adopting the classical MCC model for the soil. Although this critical state model is capable of capturing the essential features of soft, lightly overconsolidated clays, it fails to reproduce the behavior of natural structured clays, characterized by the presence of intergranular bonds of various origin. To investigate the effects of bonding on the soil response to the piezocone advancement, in this work the isotropic hardening elastoplastic model for natural, structured soils proposed by Nova and coworkers (Tamagnini et al. 2002, Nova et al. 2003) has been extended to finite deformations adopting a multiplicative decomposition of the deformation gradient into elastic and plastic parts (see, *e.g.*, Borja & Tamagnini 1998). The finite deformation plasticity model thus obtained - referred to in the following as the FD_Milan model - has been implemented in a geomechanics-oriented PFEM code (G–PFEM, Monforte et al. 2017) and has been used in this work to simulate CPTu tests in a relatively soft natural clay.

The remainder of the paper is as follows. A brief overview of the FD_Milan model is provided in Sect. 2, while the details of the CPTu simulations program are given in Sect. 3. A selection of the results obtained in the PFEM simulations is presented in Sect. 4. Sect. 5 provides the main concluding remarks and suggestions for further studies.

2 THE FD_MILAN MODEL

2.1 *Local version*

The FD_Milan model is a non-associative, isotropic hardening finite-deformation plasticity model for structured soils and weak rocks, developed by Oliynyk et al. (2021) based on the multiplicative decomposition of the deformation gradient and on the adoption of a suitable free energy function to describe the elastic response of the material. Its evolution equations in the spatial setting are briefly summarized here:

$$\overset{\nabla}{\boldsymbol{\tau}} = \mathbf{a}^e(\boldsymbol{d} - \boldsymbol{d}^p)\,(\text{hyperelastic eq.}) \tag{1}$$

$$\boldsymbol{d}^p = \dot{\gamma}\frac{\partial g}{\partial \boldsymbol{\tau}}\,(\text{flow rule}) \tag{2}$$

$$\dot{P}_s = \dot{\gamma}\rho_s P_s\big(\hat{V} + \xi_s\hat{D}\big)\,(\text{hardn. law for } P_s) \tag{3}$$

$$\dot{P}_t = -\dot{\gamma}\rho_t P_t\big(|\hat{V}| + \xi_t\hat{D}\big)\,(\text{hardn. law for } P_t) \tag{4}$$

subjected to the Kuhn-Tucker complementarity conditions:

$$f(\boldsymbol{\tau}, P_s, P_t) \le 0 \quad \dot{\gamma} \ge 0 \quad \dot{\gamma} f(\boldsymbol{\tau}, P_s, P_t) = 0 \tag{5}$$

In the above equations, $\boldsymbol{\tau}$ and $\overset{\nabla}{\boldsymbol{\tau}}$ are the Kirchhoff stress and its Jaumann objective rate; d is the rate of deformation tensor; $\boldsymbol{d}^p$ is the plastic rate of deformation tensor; $\mathbf{a}^e$ is the spatial hyperelastic tangent stiffness of the material; $\dot{\gamma}$ is the plastic multiplier; f and g are the yield function and the plastic potential, respectively (see Oliynyk et al. 2021 for details); P_s and P_t are internal variables; the functions

$$\dot{\gamma}\hat{V} = \dot{\gamma}\ \mathrm{tr}\left(\tfrac{\partial g}{\partial \boldsymbol{\tau}}\right) \quad \dot{\gamma}\hat{D} = \dot{\gamma}\sqrt{\tfrac{2}{3}}\left\|\mathrm{dev}\left(\tfrac{\partial g}{\partial \boldsymbol{\tau}}\right)\right\|$$

are the plastic volumetric and deviatoric rates of deformation; and ρ_s, ξ_s, ρ_t and ξ_t are material constants.

The first internal variables P_s (*preconsolidation pressure*) accounts for the hardening/softening effects due to volumetric and deviatoric plastic strains. The second, P_t (*bond strength*), quantifies the effects of material structure (fabric and bonding). A representation of the yield surface in the Kirchhoff stress invariants space P:Q, highlighting the role of the internal variables, is given in Figure 1.

For $\xi_\mathrm{s} = 0$, eq. (3) reduces to the classical volumetric hardening law of critical state soil mechanics. Plastic volumetric compaction produces an increase of P_s while plastic dilation is accompanied by a reduction of P_s.

A positive value of the bond strength P_t results in an expansion of the elastic domain in stress space. On the positive part of the P axis, the isotropic yield stress in compression is increased by a quantity $P_m = kP_t$, with k a material constant. On the negative axis, the vertex of the yield surface is displaced from the origin of the stress space to $P = -P_t$. Therefore, the structured material possesses a true cohesion and a non-negligible tensile strength. The region in the stress space contained between the actual yield surface (full black line in Figure 1) and

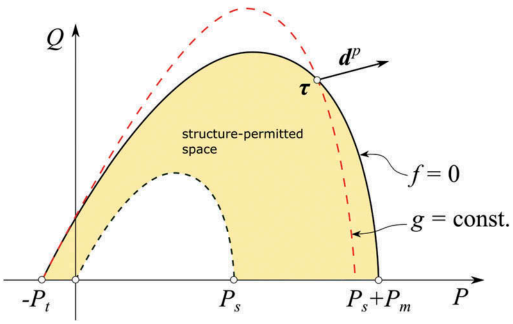

Figure 1. Yield surface and plastic potential of the FD_Milan model.

the intrinsic yield surface of the unstructured material (with $P_t = P_m = 0$, black dashed line in Figure 1), represents the so-called *structure-permitted space*, which is accessible only by the combined effects of fabric and intergranular bonding. As a consequence of the microstructural rearrangement of the soil fabric and the concurrent breakage of intergranular bonds, the structure of the material is progressively destroyed. From a macroscopic point of view, this process induces a progressive reduction of P_t with increasing accumulated plastic deformations. This process is described by the hardening law of eq. (4), in which the RHS is always negative. The final asymptotic value for P_t is zero (full destructuration): the bond-permitted space reduces to zero and the yield surface coincides with the intrinsic yield surface.

2.2 *Non-local version*

In order to provide a characteristic length scale to the constitutive equation, to regularize the numerical solution in presence of strain localization phenomena, the integral non-local approach of Oliynyk et al. (2021) has been adopted, in which the internal variables P_s and P_t are treated as non-local, spatially averaged quantities over a neighborhood Ω of the material point. The size of this neighborhood is controlled by a material constant ℓ_c, called *characteristic length*.

Let us rewrite the hardening laws (3) and (4) in the following equivalent integrated form:

$$P_s = P_{s0} \exp\{\rho_s(-E_v^p + \xi_s E_s^p)\} \tag{6}$$

$$P_t = P_{t0} \exp\{-\rho_t(N_v^p + \xi_t E_s^p)\} \tag{7}$$

where E_v^p, E_s^p and N_s^p are three strain-like internal variables, whose evolution equations are provided by:

$$\dot{E}_v^p = \dot{\gamma}\hat{V} \quad \dot{E}_s^p = \dot{\gamma}\hat{D} \quad \dot{N}_v^p = \dot{\gamma}|\hat{V}| \tag{8}$$

and P_{s0} and P_{t0} represent the initial values of the internal variables. Once E_v^p, E_s^p and N_v^p are chosen as alternative state variable, their values can be spatially averaged in a neighborhood Ω of each material point $x = \phi(X,t)$ at time t. The spatial averages are computed numerically by the following expressions:

$$\overline{A}(\boldsymbol{x}_i) = \frac{1}{\sum\limits_{x_j\in\Omega} w(\boldsymbol{x}_i, r_{ij})} \sum_{x_j\in\Omega} w(\boldsymbol{x}_i, r_{ij}) A(\boldsymbol{x}_j) \tag{9}$$

where the symbol A stands for one of the variables E_v^p, E_s^p or N_v^p. In eq. (9), $r_{ij} = \|x_{\mathrm{j}} - x_{\mathrm{i}}\|$ is the distance between points located at x_{j} and x_{i}, and w is a suitable weighting function, for which the expression proposed by (Galavi & Schweiger 2010):

$$w(\boldsymbol{x}, r_{ij}) = \frac{r_{ij}}{\ell_c} \exp\left\{-\left(\frac{r_{ij}}{\ell_c}\right)^2\right\} \tag{10}$$

has been adopted. The scalar quantity ℓ_c appearing in eq. (10) is a material constant providing the length scale sought after. Once the non-local quantities $\overline{E}_v^p$, $\overline{E}_s^p$ and $\overline{N}_v^p$ are known, the stress-like internal variables P_s and P_t are computed by eqs. (6) and (7).

3 SIMULATION PROGRAM

In the PFEM simulations of CPTu tests, a standard piezocone, with radius R = 1.78 cm and a cone tip angle of 60° is inserted in a calibration chamber with radius B = 0.45 m and height H = 1.05 m, filled with a fully saturated clay. The problem has been assumed as axisymmetric. A sketch of the problem geometry along with some snapshots of the spatial adaptive PFEM discretization at 3 different tip advancement depths is given in Figure 2.

The piezocone is wished-in-place at an initial depth z_0 = 0.25 m and then displaced downwards at a constant penetration speed of 2.0 cm/s, up to a depth $z = z_0 + 20R$. The piezocone tip and its lateral surface are modeled as rigid, impervious surfaces, and a smooth contact interface with the soil is adopted. Given the relatively small dimensions of the calibration chamber, the self weights of the pore water and of the soil have been ignored. The initial pore water pressure has been assumed uniform and equal to zero.

The material constants adopted in the simulations have been obtained by calibrating the model on the available experimental data for the Osaka clay (Adachi et al. 1995) and are reported in Table 1. The

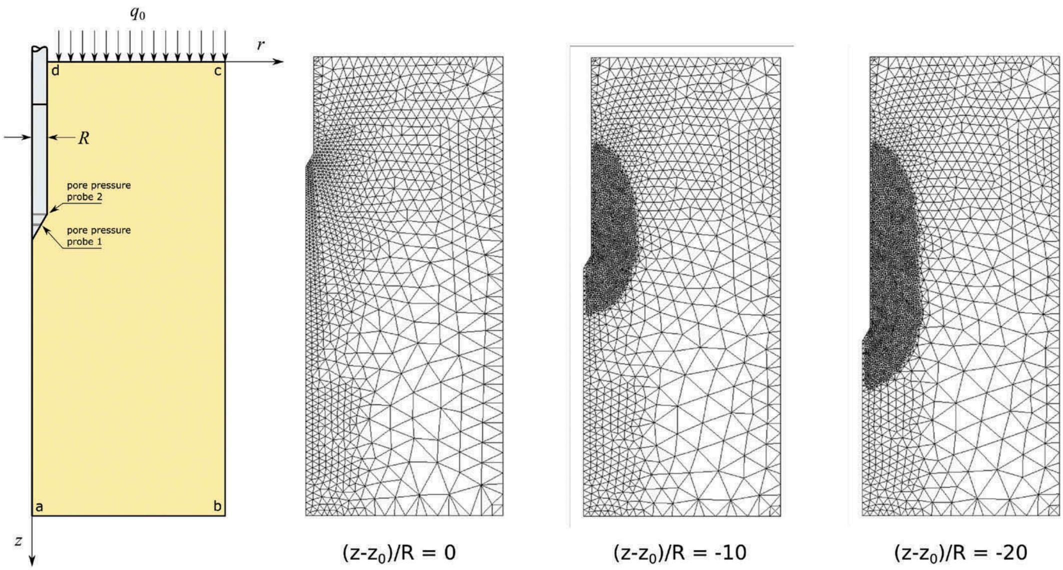

Figure 2. Problem geometry and spatial discretizations at 3 different tip advancement depths.

Table 1. Sets of material constants adopted in the CPTu test simulations (see Oliynyk et al. 2021 for details on the meaning of each constant).

$\hat{\kappa}$ (−)	G_0 (MPa)	α (−)	P_{ref} (MPa)	$M_{f,c}$ (−)	α_f (−)	μ_f (−)	$M_{g,c}$ (−)
1.82	3.0	0.0	5.0	1.1	0.75	1.50	1.1
α_g (−)	μ_g (−)	ρ_s (−)	ρ_t (−)	ξ_s (−)	ξ_t (−)	k (−)	ℓ_c (mm)
0.75	1.5	8.33	15.0	0.0	3.0	5.0	5.0

flow rule has been assumed as associative, so the plastic potential coincides with the yield function.

All the PFEM simulations have been performed as fully coupled hydromechanical problems, adopting the mixed u-Θ-p_w formulation of Monforte et al. (2017). The bottom and lateral surfaces of the calibration chamber have been assumed as rigid, impervious and perfectly rough boundaries. At the top surface of the soil body a uniform normal pressure q_0 = 100 kPa and a constant pore water pressure $p_w = 0$ have been imposed. Consistently with these boundary conditions, the initial Cauchy effective stress in the soil mass has been assumed axisymmetric, with components σ_z = 100 kPa and $\sigma_r = K_0 \sigma_z$ and K_0 = 0.5. The initial value of P_s has been set to 120 kPa.

4 SELECTED RESULTS

Six simulations have been performed considering 4 different hydraulic permeabilities, k_h, in the range 1.0e-9 to 1.0e6 m/s, and 3 different initial values for the bond strength, P_{t0}, from 0 to 60 kPa. With these initial conditions and the material properties listed in Tab. 1 the apparent peak undrained strength $c_{u,p}$ of the soil ranges from 41 to 106 kPa.

The effects of the initial degree of bonding are shown in Figures 3 and 4. The simulations reported have been performed with k_h = 1.0e-9 m/s. For such a low permeability value, the penetration process occurs in almost undrained conditions. Figure 3 shows the profiles, relative to the cases of P_{t0} equal to 0, 30 and 60 kPa, of net cone resistance, q_{n} and excess pore water pressures computed at the cone base (Δp_{w2}) and at the cone tip (Δp_{w1} as a function of the normalized penetration depth $Z = (z - z_0)/\text{R}$.

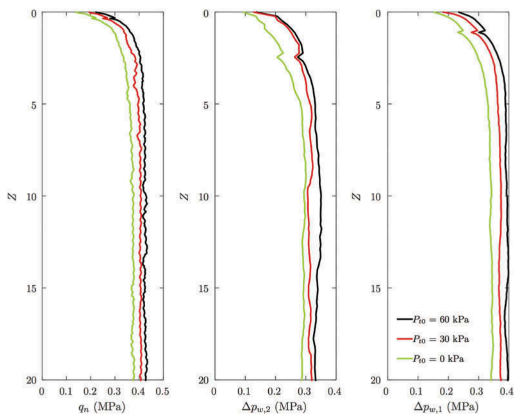

Figure 3. Profiles of net cone resistance, excess pore pressure $\Delta p_{w,2}$ and $\Delta p_{w,1}$ for different initial values of bond strength P_{t0} and k_h = 1.0e-9 m/s.

After an initial transient stage up to $Z = 5$, all the profiles reach a stationary state up to the final value of the penetration $Z = 20$. It can be observed that the stationary values of q_n, Δp_{w1} and Δp_{w2} increase with increasing P_{t0}: the higher is the initial structure of the soil, the higher are the cone resistance and the excess pore pressures developed during the cone advancement.

Figure. 4 shows a comparison of the contour maps of E^p_s, P_s, P_t and Δp_{w1} for the two extreme cases of P_{t0} = 0 and 60 kPa. In the unstructured soil, the plastic zone around the piezocone extends by about $3R$ around the shaft and the cone, with contour lines following the shape of the penetrating device. In the structured soil, on the other hand, the observed pattern of plastic shear deformations is much more irregular and show the presence of localized shear zones which originate at about $3R$ below the cone tip and bend upwards as the cone advances. The presence of shear localization is most likely due to the softening behavior associated to soil destructuration. In both cases, the preconsolidation pressure P_s is only slightly affected by the penetration process, due to the virtually undrained nature of the soil deformation. In the structured soil, the contour map of P_s highlights the presence of a region of decreasing P_s, located at the boundary of the plastic region, where plastic dilatancy is occurring. The contour map of the bond strength for the structured soil clearly indicates that, in most of the plastic region around the piezocone, the destructuration process is almost complete. Yet, the presence of structure maintains a non-negligible effect on both the cone tip resistance and the spatial distribution of the pore water pressures, as shown in the contour maps of p_w.

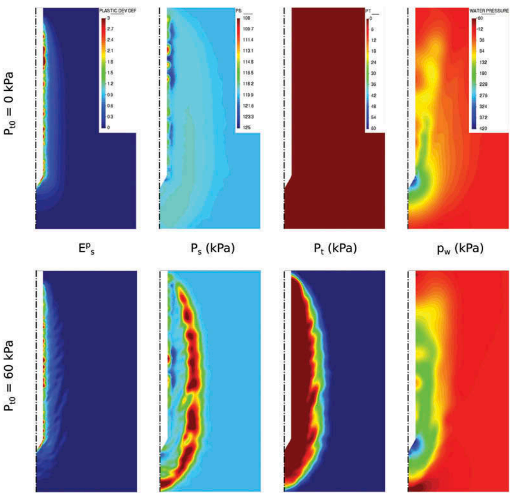

Figure 4. CPTu tests results: contour maps of E^p_s, P_s, P_t and p_w at the maximum penetration depth, for P_{t0} = 0 kPa (top) and P_{t0} = 60 kPa (bottom).

The effects of soil permeability on the predicted CPTu results are shown in Figure 5, reporting the profiles of q_n, $\Delta p_{w,1}$ and $\Delta p_{w,2}$ with Z for the four k_h values considered. From the figure, the impact of the soil permeability on the computed excess pore pressures at the two piezometers locations is immediately apparent. In the simulation with the highest permeability value the soil deforms in almost drained conditions, with a maximum Δp_w of about 50 kPa at the position of the piezometer no. 1. The maximum Δp_w are obtained at both piezometers for the lowest K_h value (1.0e-9 m/s), and only slightly smaller values of excess pore water pressure are registered at piezometer no. 2 for the next to smallest permeability. This value of k_h (1.0e-8 m/s) appears to mark the transition from fully undrained to partially drained soil response.

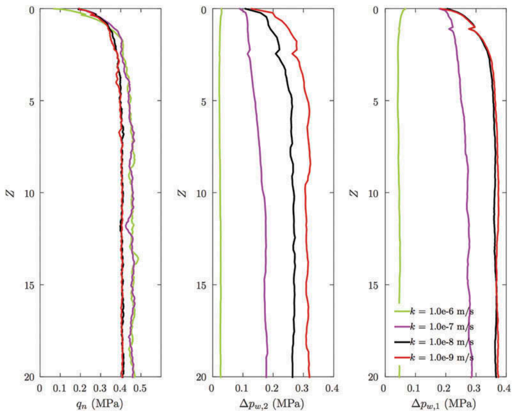

Figure 5. Profiles of net cone resistance, excess pore pressure $\Delta p_{w,2}$ and $\Delta p_{w,1}$ for different soil permeabilities and P_{t0} = 30 kPa.

As expected, the q_n profiles show a larger cone resistance in the "drained" case, as compared to the "undrained" one, with the two intermediate cases profiles remaining close to the two extremes. Surprisingly, the difference between the different profiles of q_n is not very large, being on average around 13%.

The contour maps of E^p_v in Figure 6 and of E^p_s, P_s, P_t and p_w in Figure 7, for the two limiting cases of the smallest and highest permeability values adopted, indicate that, apart from the large differences observed in the final pore water pressure fields, the collapse mechanisms around the advancing cone tip is fundamentally different in the two cases. In the "undrained" case, the plastic region around the advancing piezocone is quite large, extending for about 6R both vertically, below the cone tip, and horizontally from the piezocone axis. The plastic zone in characterized by a complex pattern of accumulated volumetric and deviatoric plastic deformations, with clearly visible bands of localized shear and volumetric deformations. On the other hand, in

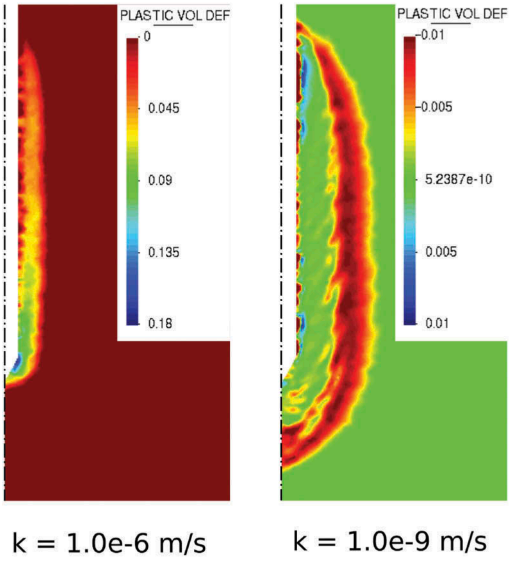

Figure 6. Contour maps of E_v^p for the maximum and minimum permeabilities considered.

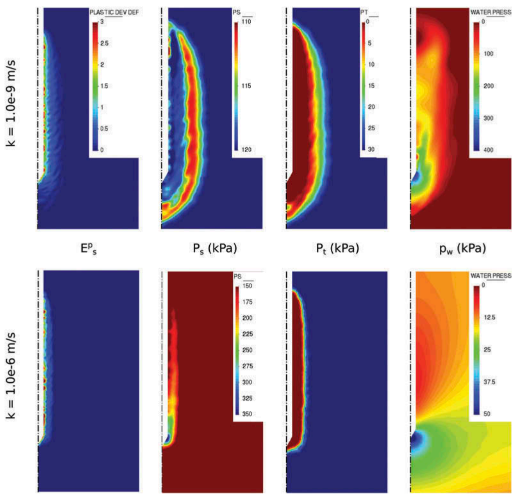

Figure 7. CPTu tests results: contour maps of E_s^p, P_s, P_t and p_w at the maximum penetration depth, for the minimum (top) and maximum (bottom) permeabilities considered.

the "drained" case, the penetration mechanism is more similar to a "punching" process, with a much smaller and homogeneous plastic zone around the cone tip and shaft. This certainly has a major effect on the stress distribution in the soil, which could explain the relatively modest differences registered in the stationary values of q_n in the two cases.

5 CONCLUDING REMARKS

The results of this preliminary study appear consistent with the observed CPTu profiles in similar soils and demonstrate that the soil response to the penetration of the piezocone in CPTu tests can actually be modeled quantitatively in a rational and computationally efficient way. The quality of the results obtained depends crucially on the capability of the constitutive model adopted to capture the essential features of the soil response during the penetration process. The FD_MILAN model presented in this work appears particularly well suited in this respect for a wide range of natural geomaterials, ranging from natural clays to porous soft rocks. The multiplicative plasticity model recently proposed by Oliynyk & Tamagnini (2020), based on the breakage mechanics, can represent a possible alternative for coarse-grained soils with crushable grains and collapsible weak rocks. The numerical simulations, performed with different initial bond strengths and soil permeabilities, show that the coupled non-linear PFEM model is capable of capturing: a) the development of plastic deformations induced by the advancement of the cone tip; b) the destructuration associated with plastic deformations; c) the space and time evolution of pore water pressure during the test. A characteristic of the plastic deformations pattern in presence of structure is the appearance of shear bands below the cone tip which propagate laterally as the tip advances and remain stationary thereafter. This feature is most likely associated to the softening mechanism induced by soil destructuration, as described by the FD_MILAN model. These results represent a promising step towards a more rational interpretation of the CPTu tests in structured geomaterials and for their use in the calibration of advanced soil models. The extension of the proposed model to incorporate thermal coupling effects (see, *e.g.*, Tamagnini and Ciantia 2016) will allow the interpretation of T-CPTu tests, which represent a promising development for the thermal characterization of soils in the design of low-enthalpy energy geostructures.

REFERENCES

Adachi, T., F. Oka, T. Hirata, T. Hashimoto, J. Nagaya, M. Mimura, & T. B. S. Pradhan (1995). Stress–strain behavior and yielding characteristics of Eastern Osaka clay. *Soils and Foundations 35*(3), 1–13.

Borja, R. I. & C. Tamagnini (1998). Cam–clay plasticity, part III: Extension of the infinitesimal model to include finite strains. *Comp. Meth. Appl. Mech. Engng. 155*, 73–95.

Carbonell, J. M., L. Monforte, M. O. Ciantia, M. Arroyo, & A. Gens (2022). Geotechnical particle finite element method for modeling of soil-structure interaction under large deformation conditions. *J. of Rock Mech. Geotech. Engng.*, http://dx.doi.org/10.1016/j.jrmge.2021.12.006.

Galavi, V. & H. F. Schweiger (2010). Nonlocal multilaminate model for strain softening analysis. *International Journal of Geomechanics 10*(1), 30–44.

Hauser, L. & H. F. Schweiger (2021). Numerical study on undrained cone penetration in structured soil using gpfem. *Computers & Geotechnics 133*, 104061.

Monforte, L., M. Arroyo, J. M. Carbonell, & A. Gens (2018). Coupled effective stress analysis of insertion problems in geotechnics with the particle finite element method. *Computers & Geotechnics 101*, 114–129.

Monforte, L., J. M. Carbonell, M. Arroyo, & A. Gens (2017). Performance of mixed formulations for the particle finite element method in soil mechanics problems. *Computational Particle Mechanics 4*(3), 269–284.

Monforte, L., A. Gens, M. Arroyo, M. Manica, & J. M. Carbonell (2021). Analysis of cone penetration in brittle liquefiable soils. *Computers and Geotechnics* 134.

Nova, R., R. Castellanza, & C. Tamagnini (2003). A constitutive model for bonded geomaterials subject to mechanical and/or chemical degradation. *Int. J. Num. Anal. Meth. Geomech. 27*(9), 705–732.

Oliynyk, K., M. O. Ciantia, & C. Tamagnini (2021). A finite deformation multiplicative plasticity model with non–local hardening for bonded geomaterials. *Comp. & Geotechnics* 137.

Oliynyk, K. & C. Tamagnini (2020). Finite deformation hyperplasticity theory for crushable, cemented granular materials. *Open Geomechanics* 2, 1–33.

O˜nate, E., S. R. Idelsohn, M. A. Celigueta, R. Rossi, J. Marti, J. M. Carbonell, P. Ryzhakov, & B. Su´arez (2011). Advances in the particle finite element method (pfem) for solving coupled problems in engineering. In *Particle–Based Methods*, pp. 1–49. Springer.

Tamagnini, C., R. Castellanza,&R. Nova (2002). A Generalized Backward Euler algorithm for the numerical integration of an isotropic hardening elastoplastic model for mechanical and chemical degradation of bonded geomaterials. *Int. J. Num. Anal. Meth. Geomech. 26*, 963–1004.

Tamagnini, C. & M. O. Ciantia (2016). Plasticity with generalized hardening: constitutive modeling and computational aspects. *Acta Geotechnica 11*(3), 595–623.